Electronic Supplementary Material (ESI) for Chemical Communications.

Supplementary Information

A heteropolytungstate based 2D layered porous framework with high proton conductivity

Mengnan Yang, Yao Zhang, Shiyan Ji, Huafeng Li, Xinyi Ma, Yuzhen Jin, Pengtao Ma, Jingping Wang* and Jingyang Niu*

Corresponding Author

* Email: jyniu@henu.edu.cn (J. Niu); jpwang@henu.edu.cn (J. Wang)

EXPERIMENTAL SECTION

Materials and physical measurements

All chemicals were purchased commercially without further purification. Elemental analyses (C, N, and H) were recorded by means of an Elementar VarioELcube CHNS analyzer. IR spectra in the range of 400–4000 cm^{-1} were recorded on a Bruker VERTEX 70 IR spectrometer via KBr pellets. The X-ray powder diffraction (XRD) patterns were recorded with an X-ray powder diffractometer (Bruker, D8 Advance) in the 2θ angular range of 5−50° under Cu Kα radiation. Thermogravimetric (TG) analyses were performed in a N_2 atmosphere in the range of 25 to 1000 °C using a NETZSCH STA 449 F5 Jupiter thermal analyzer with a heating rate of 10 K min^{-1}. A Perkin Elmer Optima 2100 DV spectrometer was selected for inductively coupled plasma-atomic emission spectrometry (ICP-AES) analyses (Na, Ru, Bi, and W). The X-ray photoelectron spectra (XPS) were measured on a Thermo Scientific K-Alpha spectrometer with monochromatic Al as the excitation source. Electrospray ionization-mass spectrometry (ESI-MS) was determined on an ABSCIEX triple-TOF 4600 mass spectrometer.

Material Preparation: $Na_6H_4{\cdot}[\{Ru_2O(bpy)_2\}_2\{Bi_2W_{32}O_{110}\}]{\cdot}37H_2O$ ($Na_6H_4{\cdot}\mathbf{1}{\cdot}37H_2O$)

Simple raw materials $Na_2WO_4{\cdot}2H_2O$ (4.00 g, 0.012 mol) and Bi_2O_3 (0.12 g, 0.256 mmol) were dissolved in 8 mL deionized water and 4 mL 4 M hydrochloric acid respectively, the mixed solution was stirred until clarified, and then the pH of the above solution was adjusted to 4.4–5.2 with 4 M HCl. Next, $RuCl_3$ (0.20 g, 0.96 mmol) ,2,2′-

bipyridine (0.05 g, 0.32 mmol), CsCl (0.04 g, 0.23 mmol) and KCl (0.05 g, 0.67 mmol) were added to the resulting solution and stirred for 30 min, during which the solution changed from colorless to dark. The solution was stirred for 0.5 h and sealed in 25 mL Teflon-lined autoclave with heating at 433 K for 48 h. After cooling to room temperature, the solution was filtered and evaporated slowly. The black rhombic plate crystals were obtained after one week. Yield: 0.66% (0.05 g, based on Ru). Elemental analysis calcd (%) for **1**: Na, 1.52; Bi, 4.22; Ru, 4.26; W, 61.89; C, 4.68; N, 1.18; H, 1.30. Found: Na, 1.39; Bi, 4.21; Ru, 4.07; W, 59.34; C, 4.84; N, 1.13; H, 1.09. IR (KBr pellet, cm^{-1}): 3433 (br), 1632 (s), 949 (s), 811 (s), 770 (s), 659 (w), 609 (w), 479 (w).

Parallel experiments indicated that the employment of CsCl and KCl was an indispensable part of the assembling process although they were not involved in the final structure of Na_6H_4·**1**·$37H_2O$. Controlled experiments also showed that without adding these two components, or replacing Bi_2O_3 by Sb_2O_3, or changing 2,2′-bipyridine to 4,4′-bipyridine, the title compound could not be obtained, but lots of colorless crystals were identified as paratungstate $[H_2W_{12}O_{42}]^{10-}$ over the entire evaporation period.

Proton conduction process

Step one, the single crystals were uniformly ground into powder and then were put into a homemade mold with a radius of 0.15 cm to obtain circular pellets. The thickness was measured by a vernier caliper. And the thicknesses of the Na_6H_4·**1**·$37H_2O$ sample was 1.22 mm. Step two, both sides of the pellets were coated with silver glue and dried naturally in air. Step three, the pellets were fixed on the sample stage with gold wires.

The proton conductivities were measured using a Solartron 1260 impedance/gain-phase analyzer with a Solartron 1296 dielectric interface (Ametek, UK) through the quasi-four-probe method over a frequency range from 0.1 Hz to 10 MHz within the input voltage of 100 mV. The measurements were operated at the temperatures ranged from 298 to 358 K, and the RHs from 35 to 85%. The impedances at each temperature were tested after equilibration for 2 h. The proton conductivity (σ) of the sample is calculated according to the Nyquist plot and the following equation:

$$\sigma = \frac{L}{SR}$$

where L and S are the length (cm) and cross-sectional area (cm^2) of the pressed plate, respectively, and R is the bulk resistance of the sample (Ω), which was extracted from the Nyquist plots. The activation energy (Ea) was calculated using the following equations:

$$ln\,\sigma T = ln\,\sigma_0 - \frac{Ea}{kT}$$

$$k = 8.6 \times 10^{-5} eVK^{-1}$$

where σ is the conductivity (S cm^{-1}), K is the Boltzmann constant (eV K^{-1}), and T is the temperature (K).

X-ray Crystallography

Some suitable shapes crystal with appropriate size were selected and placed on a Bruker D8 VENTURE PHOTON II CCD diffractometer. The radiation source of graphite-monochromated Mo Kα (λ = 0.71073 Å) was used to collect the crystal data in the cooled nitrogen flow at 150 K. The SHELXT structure solution program was used to solve all the structures, and the SHELXL refinement package in Olex2 was used for the

full-matrix least-squares algorithm on F^2 data. In the final refinement cycle, the C, O, Bi, Ru, W, N, and Na atoms were refined into anisotropy. The assignment of water molecules was supported by the IR spectra and TG results. Placing the hydrogen atoms from the organic ligands in the calculated position. CCDC contains the supplementary crystallographic data for this paper with deposition number 2270810 for Na_6H_4·**1**·$37H_2O$. The crystallographic data can be obtained free of charge from The Cambridge Crystallographic Data Center via http://www.ccdc.cam.ac.uk/data_request/cif. **Table S1** shows the crystallographic data and structural refinement parameters for Na_6H_4·**1**·$37H_2O$.

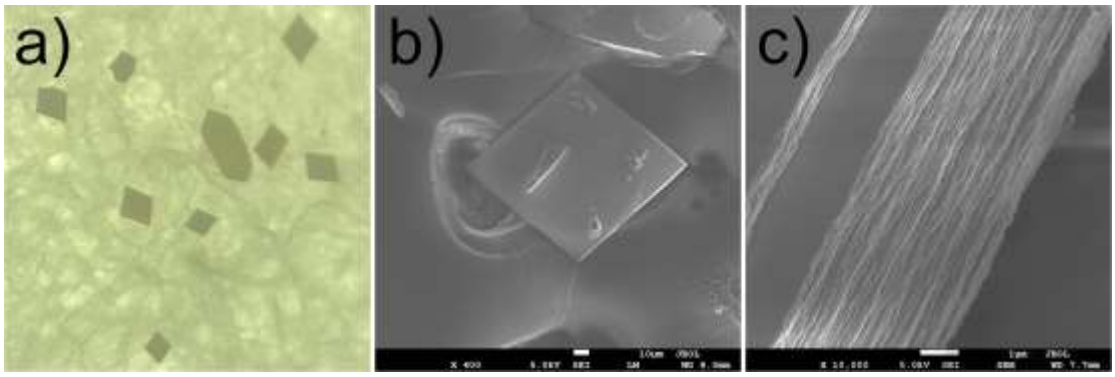

Fig. S1 (a) Microscopic image of rhombic plate crystals of Na_6H_4·**1**·$37H_2O$, and (b, c) SEM images under various magnifications.

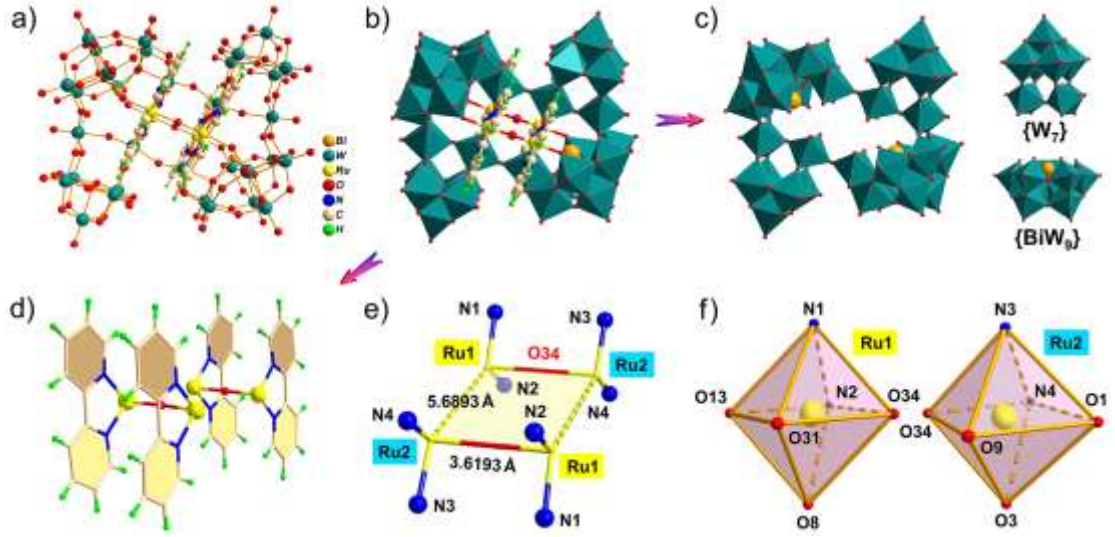

Fig. S2 (a) Ball-and-stick representation and (b) polyhedral representation of cluster anion **1**; (c) an inorganic polyoxoanion $\{Bi_2W_{32}\}^{22-}$ consist of centrosymmetric two pairs of $\{\beta\text{-B-}BiW_9O_{33}\}^{9-}$ (BiW_9) and $\{W_7O_{22}\}^{2-}$ (W_7) secondary units, and (d) two organic-hybrid-ruthenium $\{Ru_2O(bpy)_2\}^{6+}$ centre linkages in cluster **1**; (e) composition plan and (f) coordination environment of the Ru1 and Ru2 heteroatoms with the bpy ligands. Color code: C (tan), O (red), N (blue), H (green), W (teal), Bi (orange), Ru (yellow), and WO_6 octahedra (teal).

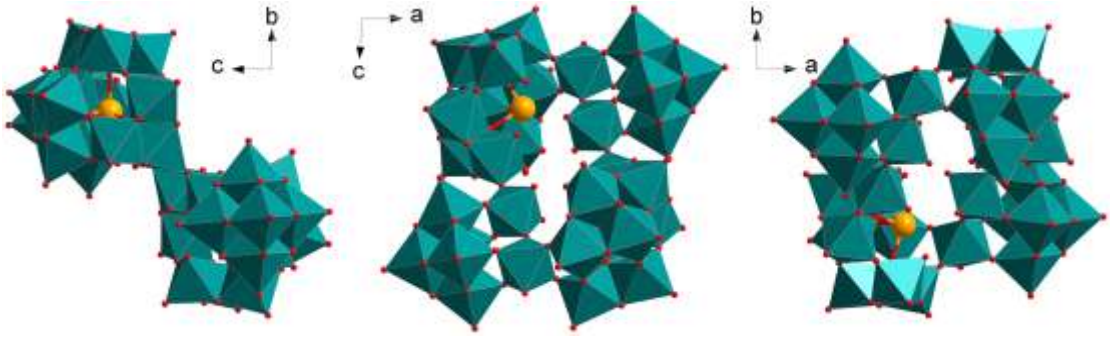

Fig. S3 Polyhedral representation of inorganic polyoxoanion $\{Bi_2W_{32}\}$ exemplified along three crystallographic axes.

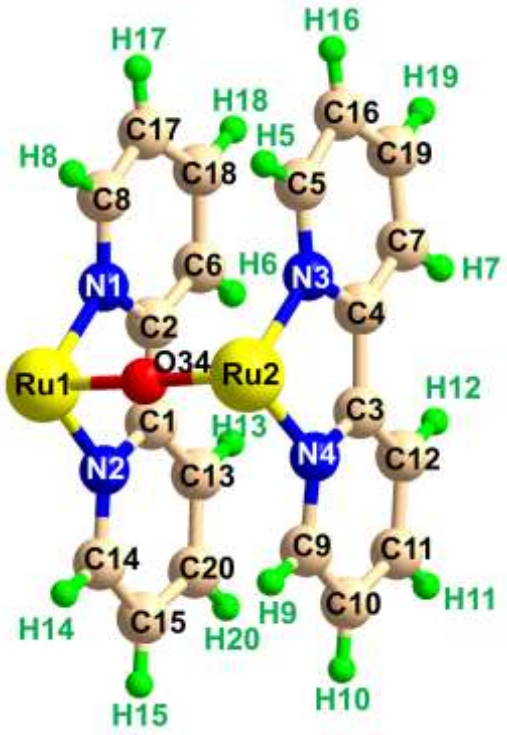

Fig. S4 Ball and stick representation of organic-hybrid-ruthenium $\{Ru_2O(bpy)_2\}$ centre linkage in cluster **1**.

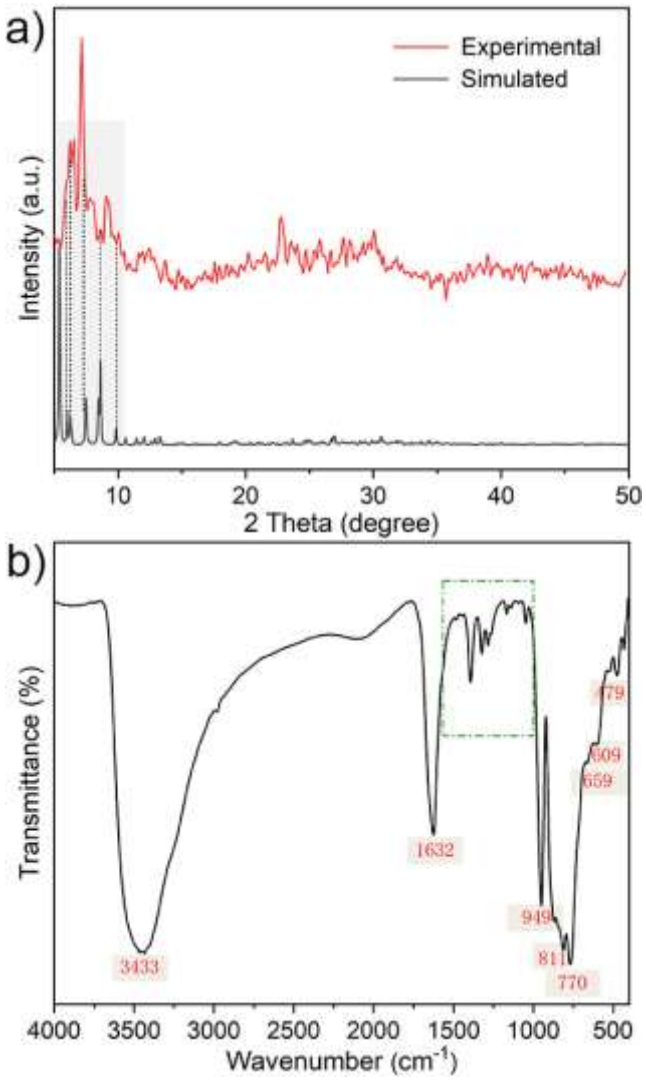

Fig. S5 (a) Simulated and experimental XRD patterns; (b) IR spectrum of Na_6H_4·**1**·$37H_2O$.

The main diffraction peaks of the experimental XRD pattern of Na_6H_4·**1**·$37H_2O$ agree with the simulated pattern, implying its good crystalline phase purity (**Fig. S5**a). The IR spectra (**Fig. S5**b) show the characteristic absorption peaks at about 949, 811, 770, and 659 cm^{-1} attributed to the vibrations of ν(W–O_b–W), ν(Bi–O_a), ν(W–O_d), and ν(W–O_c), respectively.[1] The vibration peaks observed at 3433 and 1632 cm^{-1} are ascribed to the adsorbed and crystal water.[2] The band at 1000–1500 cm^{-1} belongs to the vibration of bpy ($C_{10}H_8N_2$) ligands.

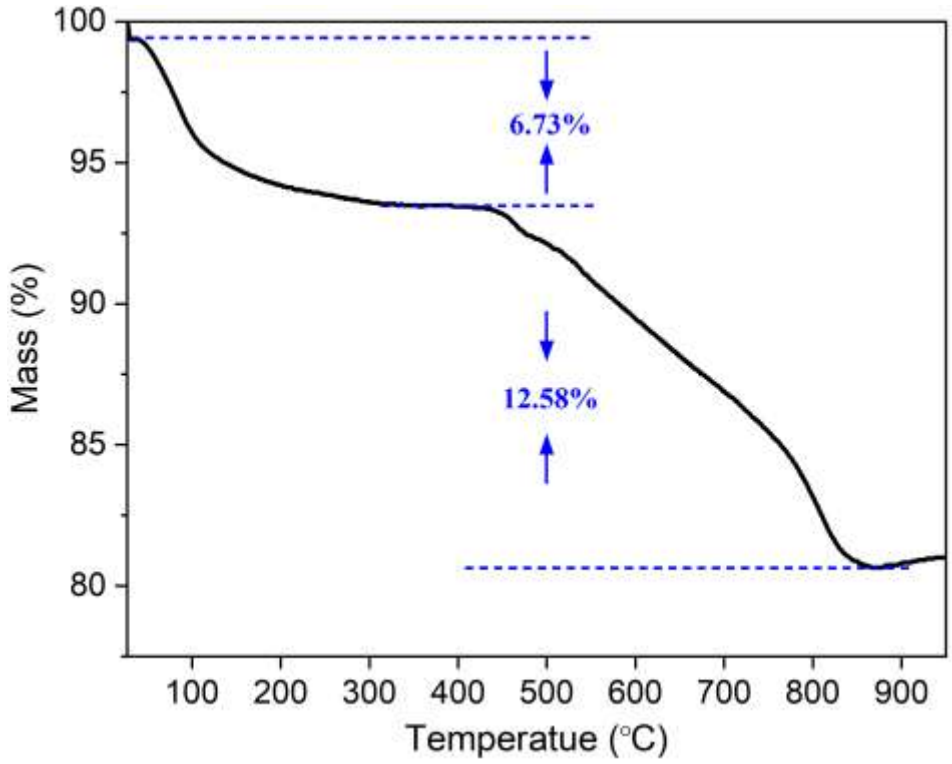

Fig. S6 Thermogravimetric (TG) curve of Na_6H_4·**1**·$37H_2O$.

The weight changes of compound Na_6H_4·**1**·$37H_2O$ in N_2 atmosphere (**Fig. S6**) exhibit two-step weightlessness of 6.73% (30–440 °C) mainly due to the loss of thirty-seven crystal water molecules (the calculated equation is seen in our previous work), and 12.58% at 440–800 °C assigned to the decomposition of cluster·**1** skeleton and the oxidation of bpy ligands.

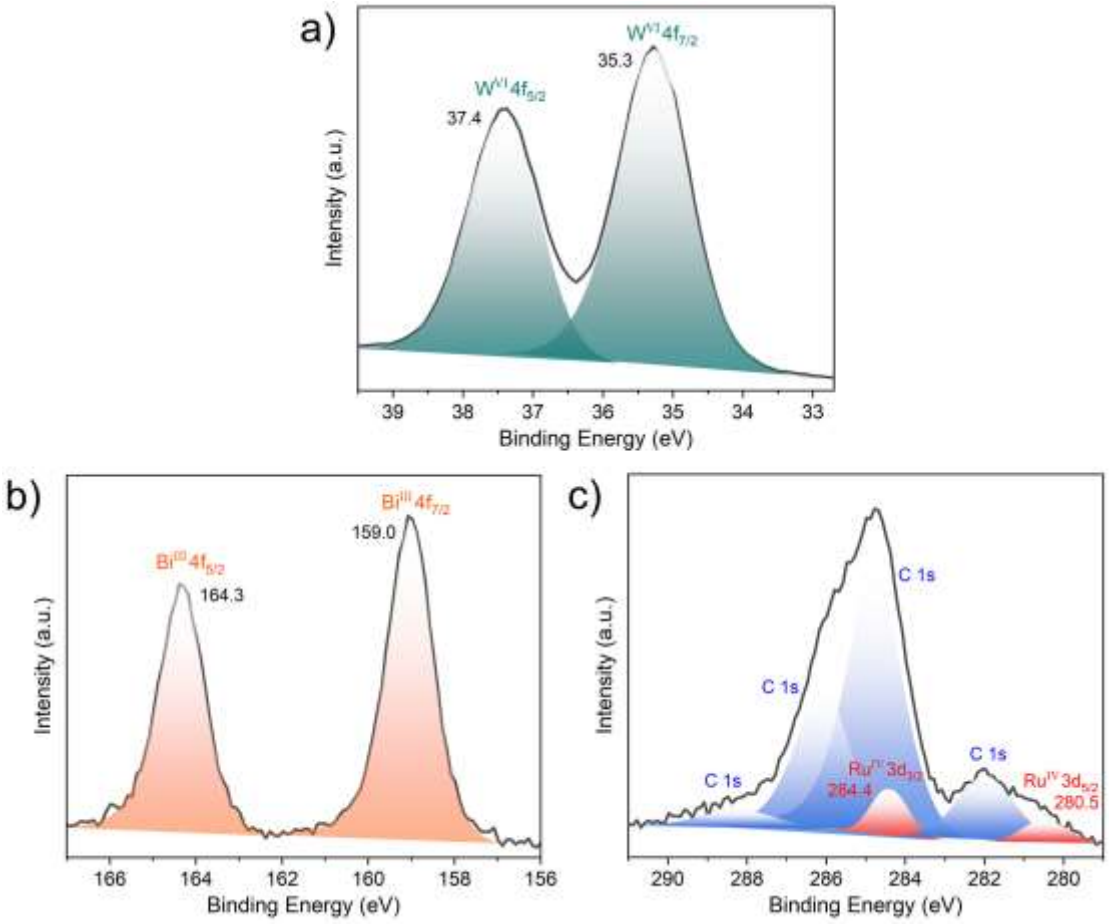

Fig. S7 (a) W 4f, (b) Bi 4f, and (c) Ru 3d XPS spectra for the fresh sample of Na_6H_4·**1**·$37H_2O$.

High-resolution XPS spectra of W 4f, Bi 4f, and Ru 3d were recorded to further verify the valence states of cluster·**1**. The XPS peaks of W 4f were observed at binding energies of 37.4 and 35.3 eV, corresponding to W $3d_{5/2}$ and W $3d_{7/2}$ of W^{VI} (**Fig. S7**a).[3] Meanwhile, the Bi 4f spectra (**Fig. S7**b) showed the peaks at 159.0 and 164.3 eV ascribed to Bi $4f_{7/2}$ and Bi $4f_{5/2}$ of the Bi^{III} oxidation state.[4, 5] The Ru 3d spectra in **Fig. S7**c presented the peaks at 284.4 and 280.5 eV attributed to Ru $3d_{3/2}$ and Ru $3d_{5/2}$ of Ru^{IV}.[6] Thus, the XPS results supported the BVS calculations of cluster·**1** in **Table S2**.

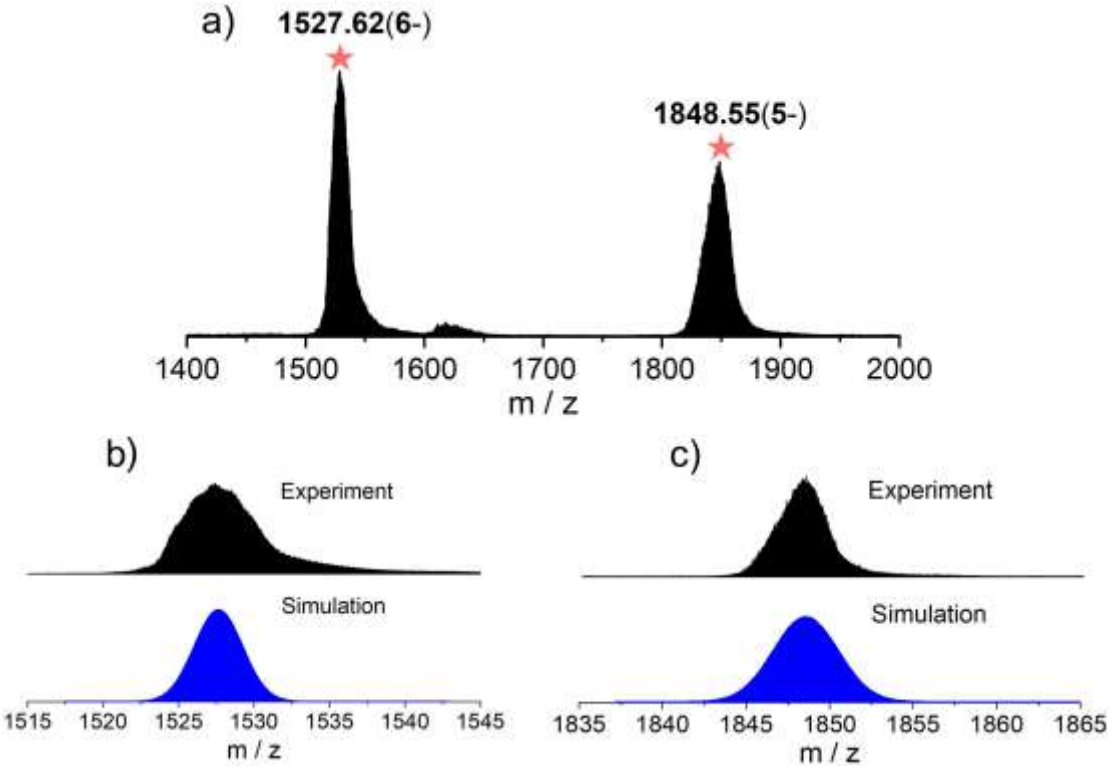

Fig. S8 (a) The ESI-MS spectrum corresponding to the intact cluster; the simulated (blue) and experimental (black) patterns at around m/z (b) 1527.62, and (c) 1848.55.

To investigate the solution behaviour, cluster **1** was monitored utilizing high-resolution electrospray ionization mass spectrometry (ESI-MS) in aqueous solution (**Fig. S8**). The negative-ion ESI-MS showed two major peaks at m/z 1527.62 (simulated 1527.64) and 1848.55 (simulated 1848.57) with charges of −6 and −5, belong to $[Na(H_2O)H_3\{Ru_2O(bpy)_2\}_2\{(W_7O_{22})(BiW_9O_{33})\}_2]^{6-}$ and $[Na_2(H_2O)_4H_3\{Ru_2O(bpy)_2\}_2\{(W_7O_{22})(BiW_9O_{33})\}_2]^{5-}$, respectively. It demonstrated that compound **1** remained intact as a cluster anion in aqueous solution, indicating its structural stability.

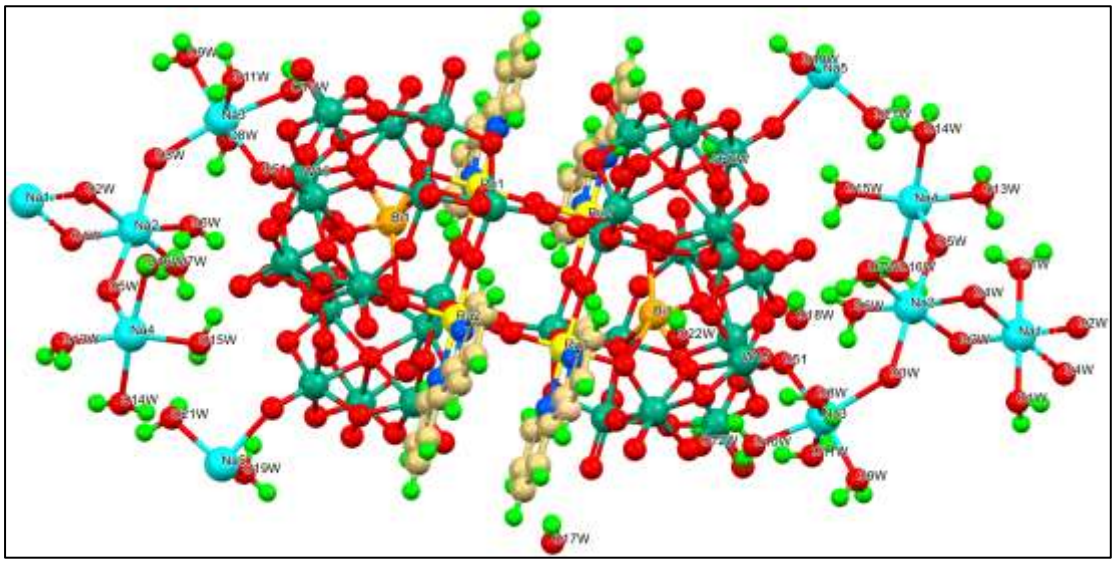

Fig. S9 Na cations (**Na1–5**) and crystal waters represented as **O(1–22)W** in the crystal chemical unit of cluster anion **1**.

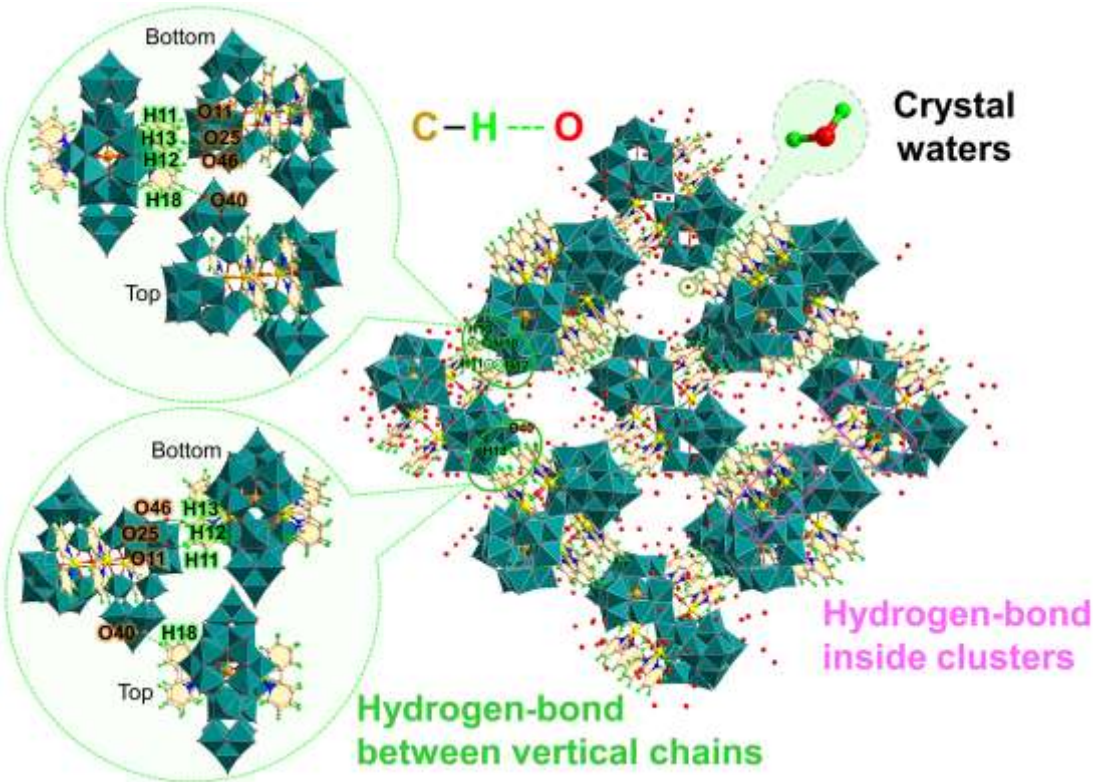

Fig. S10 Weaving Na-bridged cluster chains into a layered porous framework through C−H···O hydrogen bonds between bpy ligands and inorganic polyoxoanions of vertical chains (for details see **Table S6**); therefore, forming the pore walls rich in crystal waters (O(1–22)W) coordinated to the Na cations and hydrogen bond interactions of C−H···O−W.

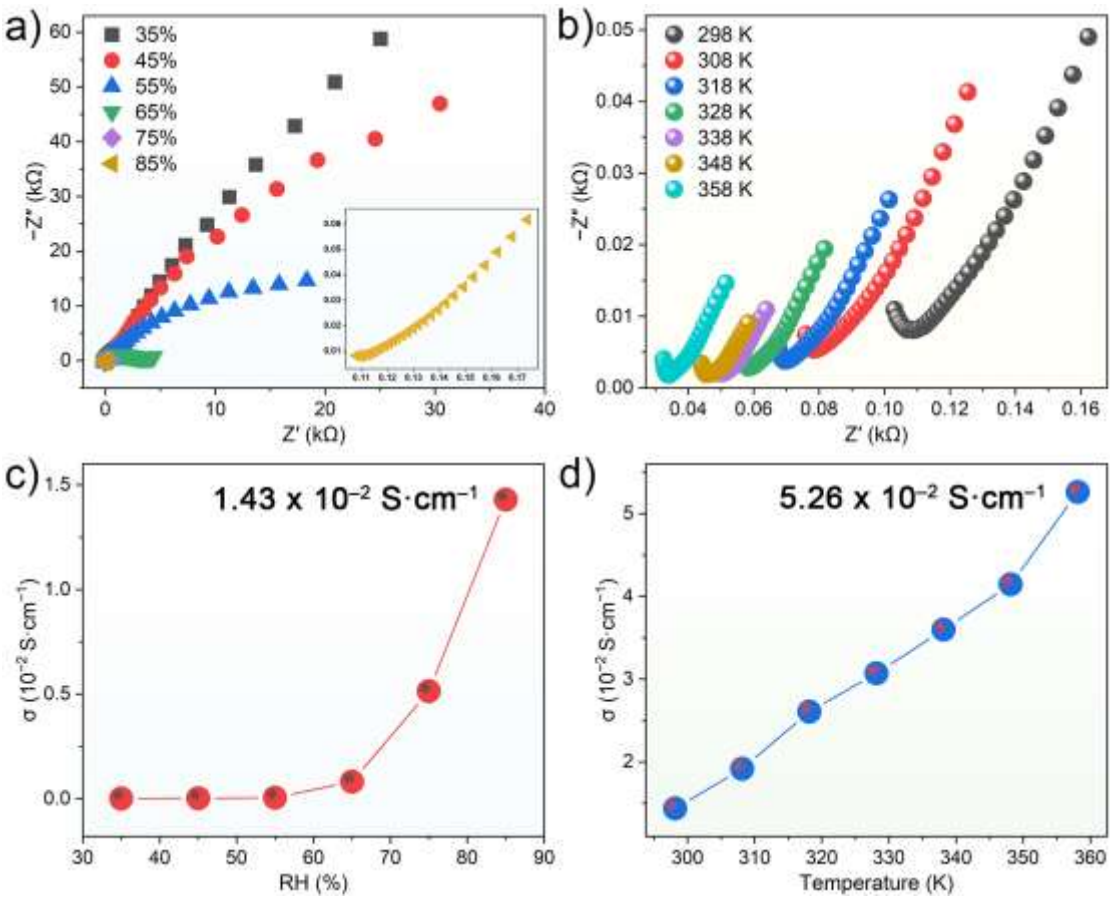

Fig. S11 Nyquist plots of Na_6H_4·**1**·$37H_2O$ (a) under different RHs at 298 K, and (b) at 85% RH under different temperatures; (c) RH-dependent and (d) temperature-dependent proton conductivities.

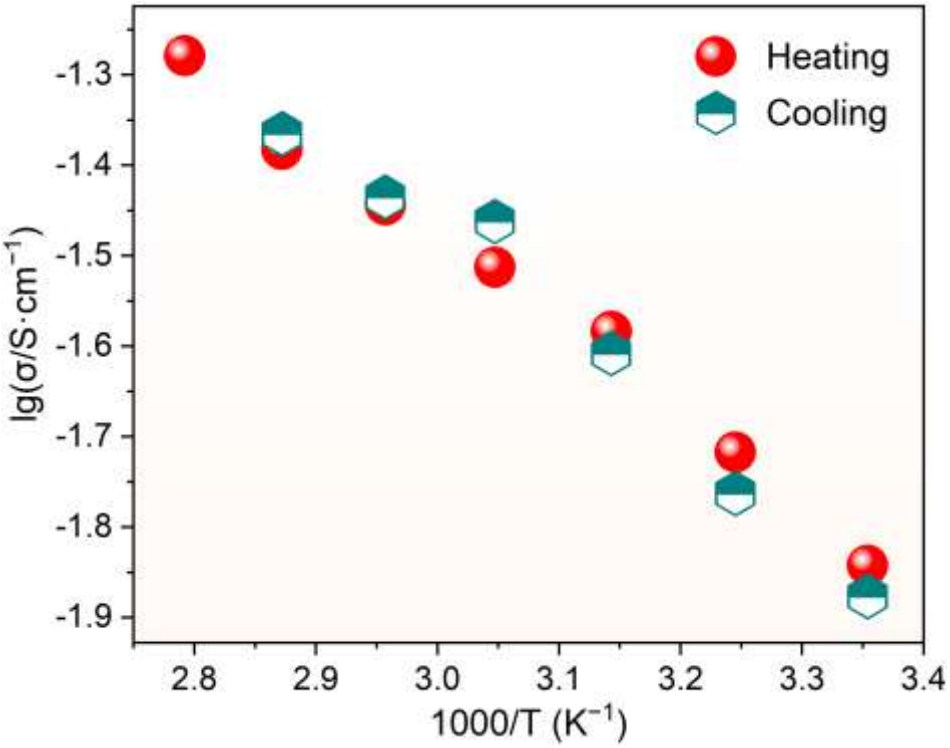

Fig. S12 Log-scaled proton conductivities for the heating-cooling cycle at 85% RH.

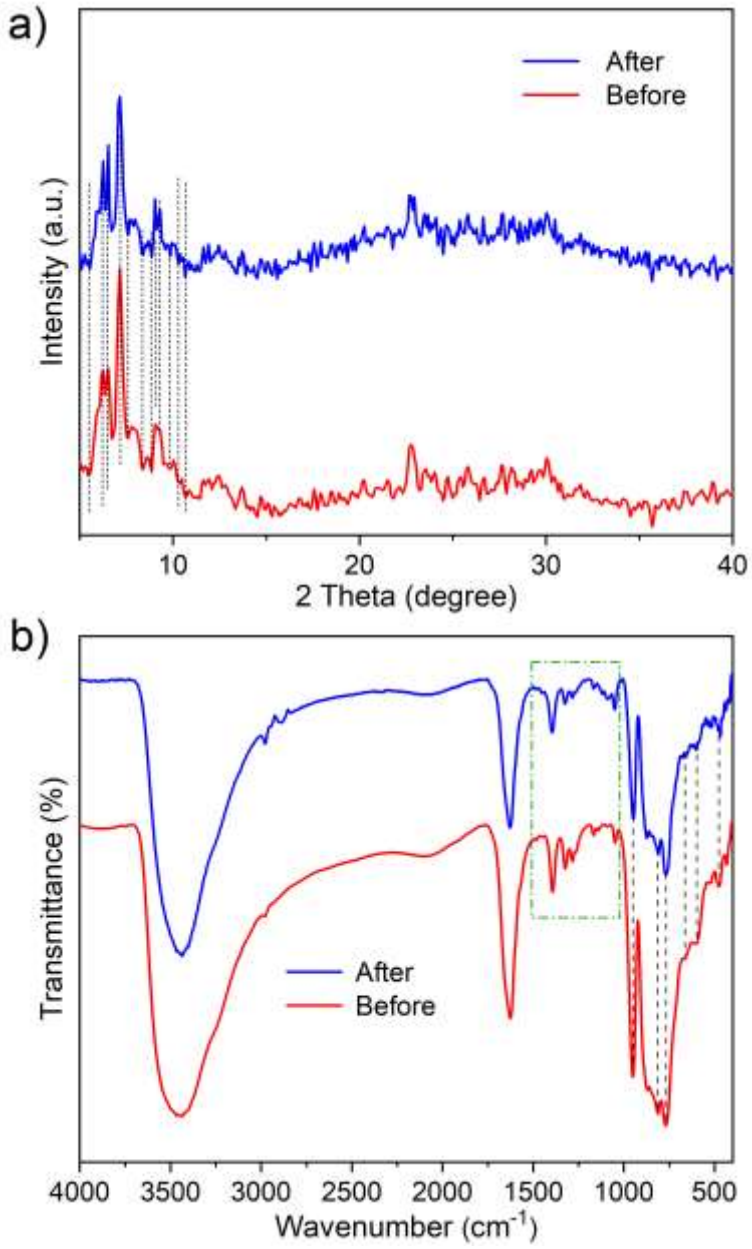

Fig. S13 (a) XRD patterns and (b) IR spectra of $Na_6H_4 \cdot \mathbf{1} \cdot 37H_2O$ before and after the proton conductivity measurement.

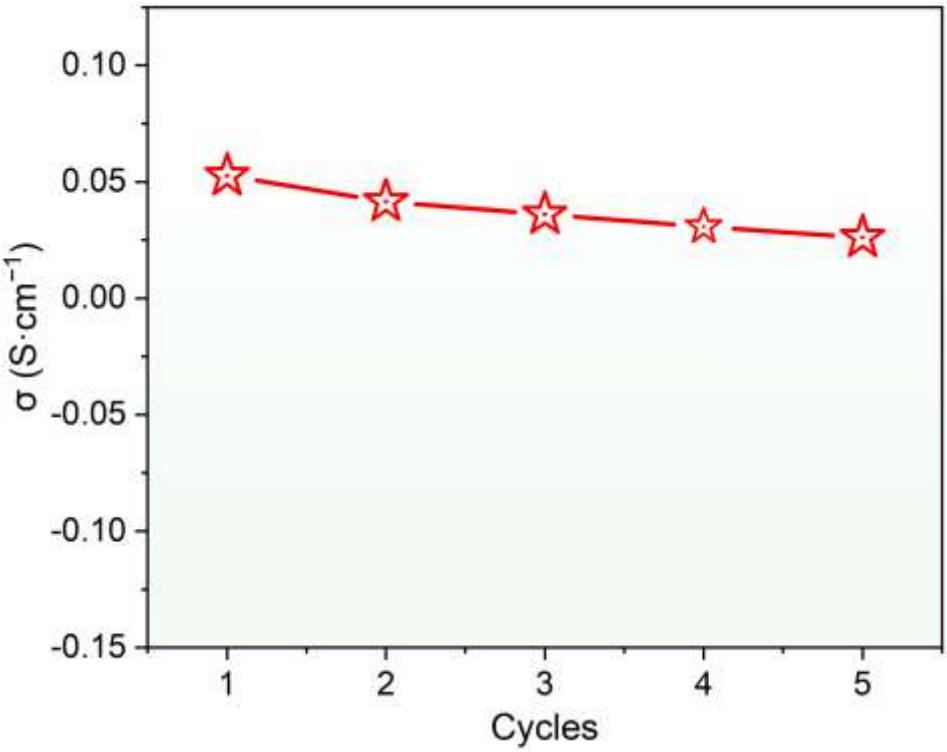

Fig. S14 Stability of proton conductivity at 358 K and 85% RH for five cycles.

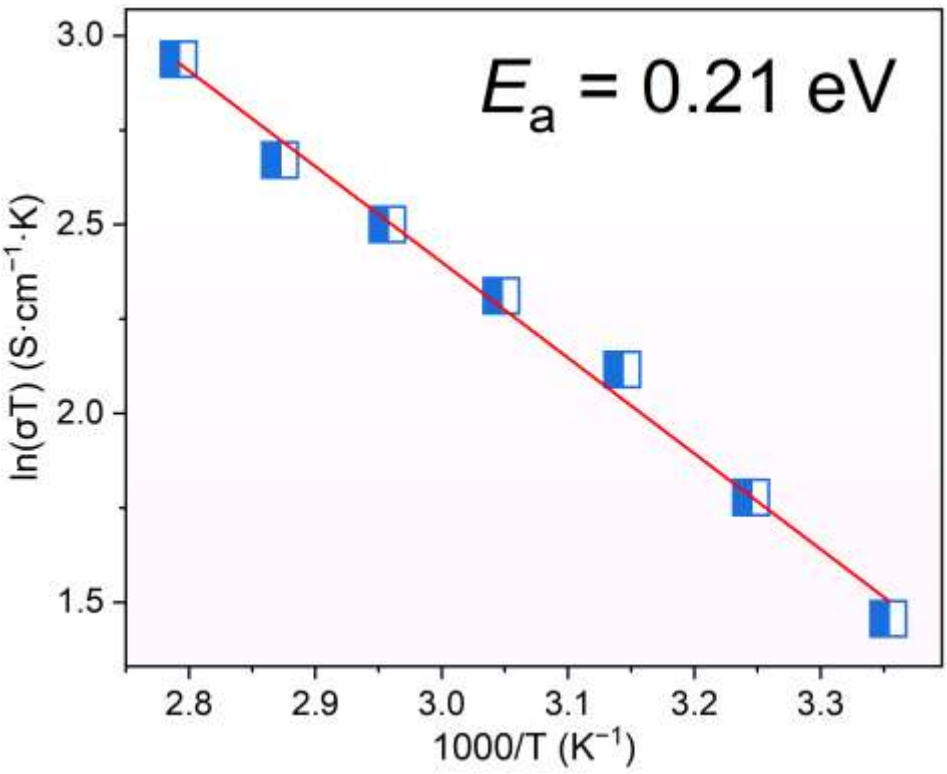

Fig. S15 Arrhenius plots of Na_6H_4·**1**·37H_2O and linear fitting at 85% RH.

Table S1 Crystal data and structure refinements for compound Na_6H_4·**1**·$37H_2O$.

Compound	Na_6H_4·**1**·$37H_2O$
Formula	$C_{40}H_{32}Bi_2N_8Na_6O_{145}Ru_4W_{32}$
M	9788.11
λ/Å	0.71073
T/K	150 K
Crystal dimensions/mm	0.1 × 0.08 × 0.07
Crystal system	monoclinic
Space group	$P2_1/n$
a/Å	17.9756(4)
b/Å	22.7835(7)
c/Å	23.5537(6)
α (°)	90
β (º)	93.4190(10)
γ (º)	90
V/Å^3	9629.2(4)
Z	2
D_c/Mg m^{-3}	3.376
μ/mm^{-1}	21.256
F(000)	8528.0
2θ Range/°	4.524 to 50.198
Data/restraints/parameters	17126/24/1132
$R_1(I > 2\sigma(I))^a$	0.0399
wR_2 (all data)^b	0.1047
Goodness-of-fit on F^2	1.019

[a] $R_1=\Sigma||F_o|-|F_c||/\Sigma|F_o|$. [b] $wR_2=\{\Sigma[w(F_o^2-F_c^2)^2]/\Sigma[w(F_o^2)^2]\}^{1/2}$

Table S2 BVS values of Ru, Bi, W, and selected O atoms of compound Na_6H_4·**1**·37H_2O.

Atom	BVS	Atom	BVS	Atom	BVS	Atom	BVS
Ru1	4.444	Ru2	4.551	Bi1	2.717	W1	6.352
W2	6.084	W3	6.083	W4	6.013	W5	6.014
W10	6.078	W11	6.091	W12	6.159	W13	6.150
W14	5.964	W15	6.077	W16	6.166	O1	1.920
O2	1.463	O3	2.122	O4	2.021	O5	2.136
O10	1.768	O11	1.924	O12	2.097	O13	1.941
O14	1.828	O15	1.976	O16	1.998	O17	1.970
O22	2.042	O23	1.894	O24	1.809	O25	2.005
O26	2.003	O27	1.853	O28	1.908	O29	1.862
O30	1.832	O31	2.094	O32	1.613	O33	1.877
O34	2.361	O35	2.022	O36	1.941	O37	1.919
O50	1.754	O51	2.492	O52	1.730	O53	1.671
O54	1.680	O55	1.626	O56	1.861		

Table S3 Selected bond distances of compound $Na_6H_4 \cdot \mathbf{1} \cdot 37H_2O$.

$Na_6H_4 \cdot \mathbf{1} \cdot 37H_2O$					
Ru1-N1	2.022 (11)	Ru2-N3	2.017 (12)	W13-O5	2.217 (8)
Ru1-N2	2.010 (11)	Ru2-N4	2.010 (11)	W13-O42	1.919 (12)
Ru1-O8	2.053 (9)	Ru2-O1	2.004 (9)	W13-O11	1.877 (9)
Ru1-O13	2.009 (10)	Ru2-O3	2.020 (9)	W13-O19	1.945 (8)
Ru1-O31	2.043 (9)	Ru2-O9	2.034 (9)	W13-O36	1.919 (11)
Ru1-O34	1.811 (10)	Ru2-O34	1.806 (10)	W13-O49	1.726 (11)
W1-O2	1.776 (9)	W1-O3	1.778 (9)	W4-O17	1.942 (10)
W4-O17	1.942 (10)	W4-O21	2.307 (10)	W11-O21	2.263 (8)
W4-O23	1.934 (10)	W11-O18	1.884 (10)	W11-O40	1.956 (11)
Bi1-O5	2.136 (9)	Bi1-O10	2.135 (10)	Bi1-O12	2.121 (8)
W11-O48	1.726 (9)	W1-O8	1.750 (9)	W1-O22	2.112 (9)
W2-O4	1.792 (10)	W2-O9	1.785 (9)	W9-O10	2.226 (10)
W9-O13	1.833 (10)	W9-O15	1.973 (10)	W9-O30	1.973 (9)
W16-O10	2.285 (9)	W16-O25	1.902 (11)	W16-O52	1.727 (10)

Table S4 Selected bond angles (°) of compound $Na_6H_4 \cdot \mathbf{1} \cdot 37H_2O$.

$Na_6H_4 \cdot \mathbf{1} \cdot 37H_2O$					
O10-Bi1-O5	84.9 (4)	O12-Bi1-O5	89.7 (3)	O12-Bi1-O10	88.5 (3)
O2-W1-O3	98.3 (4)	O2-W1-O4	166.8 (4)	O2-W1-O22	89.1 (4)
O3-W1-O24	88.3 (4)	O4-W1-O22	80.4 (4)	O8-W1-O2	97.8 (4)
O8-W1-O3	101.3 (4)	O8-W1-O22	89.4 (4)	O8-W1-O24	166.8 (4)
O4-W2-O12	167.2 (3)	O4-W2-O14	97.2 (4)	O9-W2-O4	102.6 (4)
O9-W2-O12	86.0 (4)	O19-W6-O2	83.8 (4)	O20-W6-O2	84.2 (4)
O28-W6-O2	82.7 (4)	O56-W6-O2	178.1 (4)	O6-W7-O12	75.3 (4)
O4-W7-O1	85.0 (4)	O4-W7-O2	165.5 (4)	O4-W7-O5	85.3 (4)
O15-W7-O6	157.8 (4)	O27-W7-O6	90.6 (4)	O35-W7-O12	86.2 (4)
O54-W7-O6	97.7 (4)	O1-W8-O5	85.9 (4)	O16-W8-O5	84.9 (4)
O29-W8-O5	74.8 (4)	O36-W8-O5	73.4 (4)	O55-W8-O1	103.2 (5)
O13-W9-O10	84.9 (4)	O15-W9-O10	84.5 (4)	O30-W9-O10	75.4 (4)
O43-W9-O10	74.4 (4)	O45-W9-O10	169.9 (5)	O26-W10-O21	75.3 (4)
O28-W10-O21	85.1 (4)	O33-W10-O21	78.2 (4)	O37-W10-O21	75.3 (4)
O50-W10-O21	174.4 (4)	O18-W11-O21	77.3 (3)	O37-W11-O21	76.2 (5)
O40-W11-O21	76.4 (3)	O41-W11-O18	91.5 (5)	O48-W11-O18	103.5 (4)
O34-Ru1-O8	92.4 (4)	O34-Ru1-N1	89.7 (4)	O1-Ru2-O3	87.5 (4)
N1-Ru1-N2	81.4 (5)	N3-Ru2-N4	80.2 (5)	Ru1-O13-W9	138.9 (5)
Ru1-O31-W2	176.0 (6)	Ru1-O8-W1	175.1 (5)	Ru2-O1-W8	138.7 (5)
Ru2-O9-W2	174.8 (6)	Ru2-O3-W1	173.3 (5)		

Table S5 Atomic parameters of Na cations, and O(1–22)W atoms represented the attached crystal waters (pink background) and isolate crystal waters (last five).

Atom	***a***	***b***	***c***
Na1	0	0.5000	0.5000
Na2	0.0306(5)	0.3849(4)	0.6044(4)
Na3	-0.0249(5)	0.4423(5)	0.7838(5)
O51	0.5281(5)	0.8329(5)	0.7181(5)
Na4	-0.0169(7)	0.2230(6)	0.4997(5)
O1W	0.0091(5)	0.4131(6)	0.4440(5)
O2W	-0.0704(5)	0.3980(4)	0.4600(4)
O3W	0.0112(7)	0.4563(7)	0.6828(6)
O4W	0.1119(6)	0.4571(6)	0.5440(6)
O5W	0.0253(9)	0.3196(9)	0.5218(7)
O6W	-0.0432(9)	0.3114(6)	0.6527(6)
O7W	0.1393(8)	0.3470(7)	0.6467(8)
O8W	0.1089(11)	0.4661(11)	0.8043(10)
O9W	-0.0658(11)	0.5391(9)	0.7889(10)
O10W	-0.0223(15)	0.4256(10)	0.8865(11)
O11W	-0.1567(15)	0.4300(14)	0.7983(14)
O13W	-0.0577(8)	0.2493(7)	0.4055(6)
O14W	0.0906(14)	0.1809(13)	0.4542(10)
O15W	0.0449(8)	0.1797(8)	0.5834(6)
O16W	-0.1175(9)	0.2620(11)	0.5532(10)

Na5	0.2404(12)	0.0782(9)	0.5511(7)
O53	0.2966(6)	0.5981(6)	0.8533(5)
O19W	0.6318(16)	0.8973(15)	0.4014(12)
O21W	0.2221(12)	0.1754(10)	0.5298(9)
O12W	-0.0572(6)	0.7020(6)	0.6529(5)
O17W	0.1721(8)	0.2353(7)	0.6236(6)
O18W	0.3646(9)	0.8526(9)	0.7330(9)
O20W	0.4716(9)	0.5227(9)	0.7958(11)
O22W	0.3849(11)	0.7729(14)	0.5880(10)

Table S6 The hydrogen bonds between vertical cluster chains (first four), and inside clusters (last four) corresponding to **Fig. S10**.

D−H···A	**d(H···A)**	**d(D···A)**	**<(DHA)**
C11−H11···O11	2.6367	3.3978	137.431
C12−H12···O25 #1	2.3603	3.0700	131.186
C13−H13···O46 #2	2.3257	3.1395	143.580
C18−H18···O40	2.6731	3.4783	142.815
C5−H5···O3 #3	2.5879	3.1662	119.476
C8−H8···O31	2.6627	3.2130	117.474
C9−H9···O9 #4	2.6525	3.2013	117.281
C14−H14···O8 #5	2.5543	3.1171	118.134

Symmetry transformations used to generate equivalent atoms: #1 x, y, z, #2 -x+1,-y+1,-z+1, #3 x, y, z, #4 x ,y, z, #5 x, y, z

Table S7 Summary of the resistance values extracted from equivalent circuit fitting of the Nyquist plots for Na_6H_4·**1**·$37H_2O$ under different RHs at room temperature, and at 85% RH under different temperatures.

Sample	RH (%)	R_{total} (ohm)	σ_{total} (ohm)
Na_6H_4·**1**·$37H_2O$	35	126101.46	1.36×10^{-5}
	45	76815.5	2.24×10^{-5}
	55	32728	5.27×10^{-5}
	65	2099.9	8.21×10^{-4}
	75	335.24	5.14×10^{-3}
	85	120	1.43×10^{-2}
	T (K)	R_{total} (ohm)	σ_{total} (ohm)
	298	120	1.43×10^{-2}
	308	90	1.91×10^{-2}
	318	66.19	2.60×10^{-2}
	328	56.2	3.07×10^{-2}
	338	47.94	3.59×10^{-2}
	348	41.62	4.14×10^{-2}
	358	32.79	5.26×10^{-2}

Table S8 Summary of proton conductive crystals based on POMs.

Compound	σ (S cm^{-1})	E_a (eV)	Conditions
$H[Ce(H_2O)_4]_2[MnV_{13}O_{38}]\cdot 9NMP\cdot 17H_2O$ [7] (3D porous framework)	4.68×10^{-3}	0.45	334 K, 97% RH
$\{Na_7[(nBu)_4N]_{17}\}[Zn(P_3Mo_6O_{29})_2]_2\ xG$ (G=guest solvent molecules) [8] (3D porous framework)	1.04×10^{-2}	0.22	353 K, 75% RH
$H_{13}(HIm)_4K_2Na_4(H_2O)_9[Sb_9SbSm_3O_{14}(H_2O)_3][(SbW_9O_{33})_3(PW_9O_{34})]\cdot 26H_2O$ [9] (1D porous framework)	1.64×10^{-2}	0.54	358 K, 98% RH
$Na_{22}\{(SbW_9O_{33})_4[La_3W_6MnO_{18}(H_2O)_8(CH_3COO)_4]_2\}\cdot nH_2O$ [10] (3D porous framework)	2.3×10^{-2}	0.327	338 K, 90% RH
$Na_{5.5}H_{6.5}[(SbW_9O_{33})_2\{WO_2(OH)\}_2\{WO_2\}RuC_7H_3NO_4]\cdot 36H_2O$ [11] (3D porous framework)	2.97×10^{-2}	0.31	348 K, 75% RH
$Na_{16}(NH_4)_{10}H_8\{[W_{14}Ce_6O_{61}]([W_3Bi_6Ce_3(H_2O)_3O_{14}][BiW_9O_{33}]_3)_2\}\cdot 38H_2O$ [12] (3D porous framework)	2.4×10^{-3}	0.677	298 K, 90% RH
3D-$\{Mo_{154}\}_n$ framework [13]	1.1×10^{-2}	0.264	295 K, 100% RH
$Na_6H_4\cdot\mathbf{1}\cdot 37H_2O$ (2D layered porous framework)	$\mathbf{1.43 \times 10^{-2}}$	0.21	298 K, 85% RH
	$\mathbf{5.26 \times 10^{-2}}$		358 K, 85% RH

NMP = N-methyl-2-pyrrolidone; Im = imidazole.

References

1 Xin X, Ma Y, Hou L*, et al.* Krebs-type $\{M_2(WO_2)_2[B\text{-}\beta\text{-}SbW_9O_{33}]_2\}^{n-}$ ($M = Sb^{III}$, (WO_3)) tungstoantimonate possessing unique pseudo-seesaw Sb–O structure. Inorg Chem, 2019, 58: 9567-9571

2 Ma P, Wan R, Si Y*, et al.* Double-malate bridging tri-lanthanoid cluster encapsulated arsenotungstates: Syntheses, structures, luminescence and magnetic properties. Dalton Trans, 2015, 44: 11514-11523

3 Feng W, Ding Y, Liu Y*, et al.* The photochromic process of polyoxometalate-based nanocomposite thin film by in situ afm and spectroscopy. Mater Chem Phys, 2006, 98: 347-352

4 Ni L, Patscheider J, Baldridge KK*, et al.* New perspectives on polyoxometalate catalysts: Alcohol oxidation with Zn/Sb-polyoxotungstates. Chem Eur J, 2012, 18: 13293-13298

5 Wang X-F, Liu X-Y, Su F*, et al.* Enhanced corrosion resistance of carbon steel in hydrochloric acid solution by polyoxometalate-estertin derivatives. ACS Omega, 2022, 7: 4429-4443

6 Zhang K, Bin D, Yang B*, et al.* Ru-assisted synthesis of Pd/Ru nanodendrites with high activity for ethanol electrooxidation. Nanoscale, 2015, 7: 12445-12451

7 Wang J-X, Wang Y-D, Wei M-J*, et al.* Inorganic open framework based on lanthanide ions and polyoxometalates with high proton conductivity. Inorg Chem Front, 2018, 5: 1213-1217

8 Gao Q, Wang X-L, Xu J*, et al.* The first demonstration of the gyroid in a polyoxometalate-based open framework with high proton conductivity. Chem Eur J, 2016, 22: 9082-9086

9 Xiao H-P, Zhang R-T, Li Z*, et al.* Organoamine-directed assembly of 5p–4f heterometallic cluster substituted polyoxometalates: Luminescence and proton conduction properties. Inorg

Chem, 2021, 60: 13718-13726

10 Wang H, Xu H, Chen C*, et al.* Parallelogram 3d-4f-5d heterometallic clusters based on trilacunary tungstoantimonates with excellent proton conductivity. Chin Chem Lett, 2023, 108486

11 Yang M, Li H, Zhang Y*, et al.* Organic hybrid antimoniotungstate layered ionic crystal: Synthesis, structure, and interlayer-confined proton conduction. Inorg Chem, 2023, 62: 6467-6473

12 Liu J-C, Han Q, Chen L-J*, et al.* Aggregation of giant cerium–bismuth tungstate clusters into a 3D porous framework with high proton conductivity. Angew Chem Int Ed, 2018, 57: 8416-8420

13 Wang H-Y, Li S-R, Wang X*, et al.* Enhanced proton conductivity of Mo_{154}-based porous inorganic framework. Sci China Chem, 2021, 64: 959-963